This article was downloaded by:
On: *25 January 2011*
Access details: *Access Details: Free Access*
Publisher *Taylor & Francis*
Informa Ltd Registered in England and Wales Registered Number: 1072954 Registered office: Mortimer House, 37-41 Mortimer Street, London W1T 3JH, UK

Liquid Crystals
Publication details, including instructions for authors and subscription information:
http://www.informaworld.com/smpp/title~content=t713926090

Mechanism of inclusion chaining in SmC* free-standing films

Philippe Cluzeau[a]; Fatiha Bougrioua[a]; Gilles Joly[a]; Lubor LejčEk Corresponding author[b]; Huu Tinh Nguyen[c]
[a] Laboratoire de Dynamique et de Structure des Matériaux Moléculaires, Université de Lille 1, 59655 Villeneuve d'Ascq Cedex, France [b] Institute of Physics, Czech Academy of Sciences, 182 21 Prague 8, Czech Republic [c] Centre de Recherche Paul Pascal, CNRS, Université de Bordeaux I, Avenue A. Schweitzer, 33600 Pessac, France

Online publication date: 25 May 2010

To cite this Article Cluzeau, Philippe , Bougrioua, Fatiha , Joly, Gilles , LejčEk Corresponding author, Lubor and Nguyen, Huu Tinh(2004) 'Mechanism of inclusion chaining in SmC* free-standing films', Liquid Crystals, 31: 5, 719 — 726
To link to this Article: DOI: 10.1080/02678290410001681564
URL: http://dx.doi.org/10.1080/02678290410001681564

PLEASE SCROLL DOWN FOR ARTICLE

Full terms and conditions of use: http://www.informaworld.com/terms-and-conditions-of-access.pdf

This article may be used for research, teaching and private study purposes. Any substantial or systematic reproduction, re-distribution, re-selling, loan or sub-licensing, systematic supply or distribution in any form to anyone is expressly forbidden.

The publisher does not give any warranty express or implied or make any representation that the contents will be complete or accurate or up to date. The accuracy of any instructions, formulae and drug doses should be independently verified with primary sources. The publisher shall not be liable for any loss, actions, claims, proceedings, demand or costs or damages whatsoever or howsoever caused arising directly or indirectly in connection with or arising out of the use of this material.

LIQUID CRYSTALS, VOL. 31, NO. 5, MAY 2004, 719–726

Taylor & Francis
Taylor & Francis Group

Mechanism of inclusion chaining in SmC* free-standing films

PHILIPPE CLUZEAU†, FATIHA BOUGRIOUA, GILLES JOLY
Laboratoire de Dynamique et de Structure des Matériaux Moléculaires,
Université de Lille 1, 59655 Villeneuve d'Ascq Cedex, France

LUBOR LEJČEK*
Institute of Physics, Czech Academy of Sciences, Na Slovance 2, 182 21 Prague 8,
Czech Republic

and HUU TINH NGUYEN
Centre de Recherche Paul Pascal, CNRS, Université de Bordeaux I,
Avenue A. Schweitzer, 33600 Pessac, France

(*Received 18 November 2003; accepted 15 January 2004*)

The self-assembly of colloidal inclusions has recently been shown in smectic C* freely suspended films. In such 2D systems, the organization of the inclusions is qualitatively explained by elastic interactions induced by the disruption of the orientational order in the SmC* host phase. The interaction between resulting inclusion–defect pairs exhibits a dipolar character. We have developed a simplified model representing every inclusion and its companion hyperbolic defect by (+1)- and (−1)-wedge disclination lines, respectively. A finite anchoring energy has been introduced to explain the coalescence of the thinnest inclusions. Our model enables us to explain the chaining of the thickest inclusions and confirms the inclusion size dependence on the stability of the chains.

Downloaded At: 16:54 25 January 2011

1. Introduction

Studies of dispersions of colloidal particles in an anisotropic host fluid have recently revealed the new phenomenon of colloidal self-assembly [1–3]. First seen in 3D emulsions of water droplets within a continuous nematic phase [1], this self-organization process results from elastic interactions mediated via the orientational order of the host phase. Competition between the boundary conditions at the droplet surfaces (e.g. radial or tangential anchoring) and the bulk elasticity of uniform nematic ordering determines the nature of the interactions and then the type of organization (e.g. in a chain, cluster, or even crystal-like structure). Experimental and theoretical studies on 3D nematic emulsions [1–7] have shown that for sufficiently strong anchoring, each droplet induces topological defect(s) (i.e. a singularity in the director field) in the nematic host phase. Depending on the symmetry of the distortion, the dominant long-range interaction is either dipolar [8] or quadrupolar [3, 4] in type. In both cases a short-range repulsive interaction due to the anchoring energy prevents the coalescence.

More recently, a similar self-organization process of colloidal inclusions was described in a 2D system consisting of smectic C* (SmC*) or smectic C (SmC) free-standing films [9–13]. In the SmC* membranes, the nucleation of cholesteric (N*) inclusions surrounded by smectic layers is induced when heating the films above the bulk SmC*–N* transition temperature [9–11]. Polarizing optical microscopy was used both for the visualization of the inclusions and the mapping of the **c**-director field (projection of the tilted molecules in the layer plane). Analysis of the texture revealed the presence of a hyperbolic defect associated with each inclusion and a radial **c**-director anchoring at the N*/SmC* boundary.

In this article, the N* droplets will be modelled by a (+1)-wedge disclination line of finite length ending in point defects located near the film surface [14], while the notion of a hyperbolic defect used in [9–11] will be expressed as a (−1)-wedge disclination line. Consequently, the pair of (±1)-disclinations and its resulting zero topological charge (by summing the (±1) charges) eliminates any director distortion at long range [14]. In § 2,

†Present address: Centre de Recherche Paul Pascal, CNRS, Université de Bordeaux I, Avenue A. Schweitzer, 33600 Pessac, France.
*Author for correspondence; e-mail: lejcekl@fzu.cz

Liquid Crystals ISSN 0267-8292 print/ISSN 1366-5855 online © 2004 Taylor & Francis Ltd
http://www.tandf.co.uk/journals
DOI: 10.1080/02678290410001681564

we will explain why the self-organization of the inclusions is mainly governed by the **c**-director distortion.

Simple solutions describing the director distribution near an isolated inclusion and its companion (-1)-wedge disclination will be developed in § 3. For that purpose we will consider the specific case of a finite molecular anchoring at the inclusion interface. In § 4, the interactions between two inclusion–defect pairs will be treated. A comparison will be made with our experimental results from [11–13]. In the last section, we will discuss the possible effects of the chirality of the smectic phase on the anchoring and the organization of the N* inclusions.

2. Elastic free energy of an SmC* liquid crystal

In this section, we discuss the contribution of the smectic layers' elasticity to the interaction between inclusions embedded in an SmC* free-standing film. As a basis we will use the general form for the free elastic energy density given in [15]. In equation (1), the first two energetic terms (A and B coefficients) describe the layer deformation, while the two last (B_1 and B_3) are related to the **c**-director distortion:

$$\rho f = \frac{A}{2}\left[2\left(\frac{\partial^2 u}{\partial x \partial y}\right)^2 + \left(\frac{\partial^2 u}{\partial x^2}\right)^2 + \left(\frac{\partial^2 u}{\partial y^2}\right)^2\right] + \frac{\bar{B}}{2}\left(\frac{\partial u}{\partial z}\right)^2 + \frac{B_1}{2}\left[\left(\frac{\partial \Phi}{\partial x}\right)^2 + \left(\frac{\partial \Phi}{\partial y}\right)^2\right] + \frac{B_3}{2}\left(\frac{\partial \Phi}{\partial z} - q\right)^2. \quad (1)$$

The coordinate system is chosen in such a way that the plane (x, y) coincides with the smectic layers, and the z-axis is normal to the layers. The layer displacement u is perpendicular to the layers. The molecular projection onto the smectic planes can be characterized by the unit director **c** in the form: $\mathbf{c} = (\cos\Phi, \sin\Phi)$ where the angle Φ characterizes the director inclination with respect to the x-axis.

The elastic constant A describes the curvature deformations of layers under the assumption of an isotropic smectic layer deformation, and $\bar{B}$ is the compressibility modulus. The parameter q is related to the SmC* helical pitch; it can be neglected in the chiral films studied provided the film thickness D is small compared with the pitch p, leading to an unwound smectic structure.

In electro-optic experiments [16] the switching of the director under an electric field parallel to the film induces negligible layer deformations. Thus, we did not take into account the coupling between the layer deformation and the director distortion in our simplified model.

According to our experimental results [11], the N* inclusions nucleate at temperatures above the bulk SmC*–N* transition. They seem to be separated from the surrounding SmC* film by a 'coat' which gives the shape of a flattened droplet to the N* inclusion, leading to a pronounced outer surface relief. The thickness of the film at the inclusion level can be up to four times greater than the background film [11]. The flattened droplet is too complex to be modelled, but it is possible to represent it in first approximation as a cylinder. The inclusion is then assimilated to a $(+1)$-wedge disclination of length h as illustrated in figure 1.

At the level of the inclusion, the smectic layers are distorted. It could be possible to model the layer deformation of the smectic film around the inclusions by a continuous distribution of prismatic dislocation loops. Each prismatic loop would correspond to an edge dislocation with a Burgers vector perpendicular to the smectic layers. The elastic energy describing the chaining of two or more inclusions via the layer distortion would then be defined by an interaction between line elements of edge dislocations. The latter is known to be proportional to the factor $\sqrt{A\bar{B}}$. Considering that we are working near to the SmC*–N* transition temperature, it is known that modulus $\bar{B}$ is almost zero [15]. As a consequence, one can expect that the contribution of the layer distortion to energy (1) can be neglected.

In the following, therefore, we will discuss only the contribution of the **c**-director deformation. Moreover, it has been assumed in expression (1) that the **c**-director rotation in the (x, y) plane is isotropic; that is, the constant B_1 represents the director deformations along both x- and y-axes. This assumption allows us to extend the use of equation (1) to cases with a large angle Φ variation in the **c**-vector field around the disclinations.

3. Solutions describing an inclusion and its hyperbolic defect

The study of SmC* films ranging from 24 to 400 smectic layers (11BSMHOB material [13]) has revealed two different behaviours during the nucleation and organization processes of the inclusions. These behaviours are clearly linked to the film thickness [11]. For

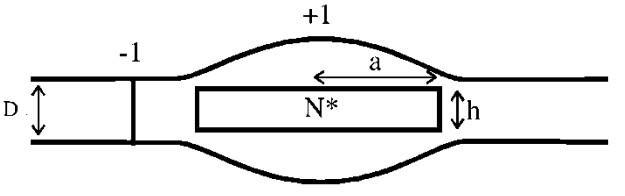

Figure 1. Schematic representation of the pair inclusion–hyperbolic defect, using a cylindrical symmetry with (± 1) topological charges. The inclusion radius is a, the film thickness D, the inclusion thickness h.

Downloaded At: 16:54 25 January 2011

the thinnest films (about 24 layers), the nucleation leads to the creation of small dispersed inclusions (with diameter 1–3 μm), which tend to coalesce with their neighbours reaching an apparent diameter of about 5 μm. In contrast, thicker films exhibit inclusions which quickly reach a diameter greater than 5 μm with no coalescence and then organize themselves into stable linear chains.

The experiments have also revealed that small inclusions exist without a visible accompanying hyperbolic defect while large inclusions have one. In the case of large inclusions, smectic molecules are anchored at the N*/SmC* interface in such a way that the **c**-director preferably adopts the radial configuration. In summary, the connection between the radial **c**-director distortion around each inclusion and the uniformity of the **c**-director field at long distance can be achieved in two ways: large inclusions induce a (−1) hyperbolic defect, while small inclusions have no visible topological defect.

Therefore we will discuss separately the cases of large and small inclusions. The modelling in [17] which was developed in the approximation of infinite anchoring can be applied to treat the behaviour of large inclusions which usually exhibit no coalescence (see § 3.1). By contrast, in the case of smaller inclusions which do coalesce, the modelling must involve a finite anchoring (§ 3.2). In § 3.3 the intermediary case of inclusions with finite but relatively high anchoring is discussed. We should note that to our knowledge no exact analytical solution is available to describe a varying anchoring energy.

Downloaded At: 16:54 25 January 2011

3.1. *Modelling with fixed anchoring*

Figure 2 gives a schematic representation of an isolated inclusion and its associated defect: a is the inclusion radius and l characterizes the distance of the hyperbolic defect from the inclusion surface. The simplest solution Φ satisfying the equilibrium Euler equation $\Delta\Phi = 0$ outside the inclusion, deduced by varying expression (1), is given in [5, 17]. The solution fulfils both the fixed radial **c**-director anchoring at the inclusion interface and the homogenous orientation at long distance. As in our notation, the defects are located along the x-axis, the solution Φ can be expressed as:

$$\Phi = 2\arctan\frac{y}{x} - \arctan\frac{(y/a)}{(x/a)-1/C} - \arctan\frac{(y/a)}{(x/a)-C} \qquad (2)$$

where the parameter $C=(a+l)/a$ introduced in [11] is denoted as the proximity coefficient. The solution (2) is composed of four disclinations: the (+1)-disclination at the centre of the inclusion represents the inclusion with the radial **c**-director organization around its cylindrical surface. The (−1)-disclination at $x = Ca$ represents the associated hyperbolic defect. A (−1)-image disclination located at $x = a/C$ describes the repulsion of the hyperbolic defect away from the inclusion surface. Finally, another (+1)-image disclination is positioned at the inclusion centre. Solution (2) is thus the system of real and image disclinations ensuring both the fixed radial anchoring at the inclusion surface and the uniform **c**-director at long distance.

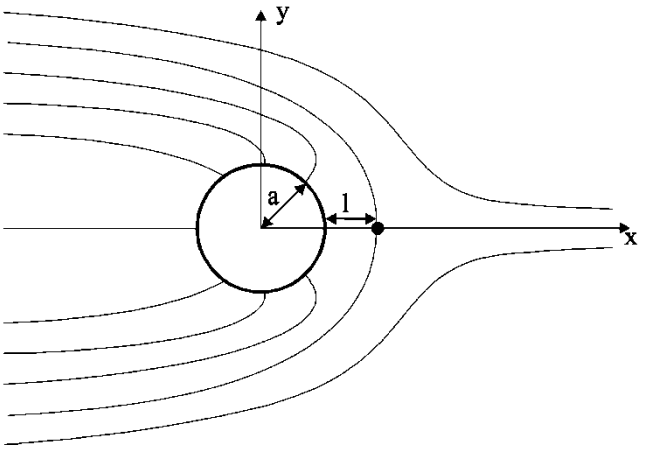

Figure 2. Isolated inclusion with (+1)-disclination and its associated hyperbolic defect with (−1)-disclination. The inclusion is centred at the origin of the coordinate system (x, y). The parameter l is the distance between its surface and the hyperbolic defect. Tangents along the solid lines depict schematically the **c**-director field which exhibits a radial anchoring at the inclusion interface.

Solution (2) is well adapted to systems with an anchoring energy at the inclusion interface sufficiently strong to keep the **c**-director orientation radial. The energetic investigation in [17], assuming a rigid anchoring at the interface, leads to an upper limit equilibrium value for the proximity coefficient $C \approx \sqrt{2}$. The interaction between inclusions with strong anchoring investigated in [17] has recently been analysed numerically [18]. Both methods seem to be in good agreement.

3.2. *Modelling with weak anchoring*

The case of small inclusions with no visible hyperbolic defects needs to be treated in the approximation of weak anchoring energy. The global uniform director orientation is locally perturbed. Solution (2) cannot be used in this case because a finite surface anchoring energy around the inclusion must be taken into account. The associated expression denoted W_A can

only be approximated by a simple form given in [19]:

$$W_A \approx -\frac{W}{2}\int_{\Sigma} dS(\mathbf{N}\,\mathbf{c})^2$$

where $\mathbf{N}=(\cos\alpha,\ \sin\alpha)$ is the normal to the phase separation surface Σ, tilted from the x-axis by an angle α.

When the surface Σ is cylindrical with radius a, the surface energy W_A (per unit length in the z-direction) can be expressed as:

$$W_A \approx -\frac{Wa}{2}\int_0^{2\pi} d\alpha \cos^2(\Phi-\alpha)|_{r=a}. \quad (3)$$

The coefficient W corresponds to the surface anchoring energy (per unit surface of inclusion) when the minimum for the energy W_A is reached: i.e. the **c**-director parallel to the surface normal ($\Phi=\alpha$). Thus Wa in equation (3) corresponds to the anchoring energy of the inclusion per unit length in the direction normal to the layers. As W is a material constant for a given compound, the anchoring energy Wa is directly controlled by the inclusion radius a.

Equations (1) and (3) lead to the condition of a finite torque at the cylindrical inclusion surface Σ:

$$a\frac{\partial\Phi}{\partial r}\bigg|_{r=a} + \frac{Wa}{2B_1}\sin 2(\Phi-\alpha)\bigg|_{r=a} = 0 \quad (4)$$

with the solution Φ satisfying the equilibrium equation $\Delta\Phi=0$ in two dimensions. We do not know the analytical solution of Φ for the problem with finite values of the parameter Wa/B_1. For this reason, in this part we first try to find an approximate solution for very small values of this factor. For this purpose, we use a modification of the method determining the director structure around a colloid particle in a nematic liquid crystal; see for example [20, 21], the numerical analysis of the similar problem is in [22]. For small values of Wa/B_1 we assume that deviations of director **c** from its uniform orientation are small, i.e. $|\Phi|\ll 1$. Then equation (4) can be rewritten as

$$a\frac{\partial\Phi}{\partial r}\bigg|_{r=a} = \frac{Wa}{2B_1}\sin 2\alpha. \quad (5)$$

The solution of the equilibrium equation $\Delta\Phi=0$, rewritten in polar coordinates (r, α) as

$$\frac{1}{r}\frac{\partial}{\partial r}\left(r\frac{\partial\Phi}{\partial r}\right)+\frac{1}{r^2}\frac{\partial^2\Phi}{\partial\alpha^2}=0$$

and satisfying (5) is then in the form:

$$\Phi = -\frac{Wa}{4B_1}\left(\frac{a}{r}\right)^2\sin 2\alpha \quad (6)$$

decreasing far away from the inclusion as $\Phi\sim(a/r)^2$. Thus solution (6) describes the director distribution for very small inclusions. Moreover, the condition $|\Phi|\ll 1$ for all $r\geqslant a$ induces $Wa/B_1\ll 4$ in (6). Note that solution (6) is equivalent to the function

$$\Phi = 2\alpha - \arctan\frac{r\sin\alpha}{r\cos\alpha-d} - \arctan\frac{r\sin\alpha}{r\cos\alpha+d} \quad (7)$$

for $d=a(Wa/4B_1)^{\frac{1}{2}}\ll a$. The solution (7) is composed of two $(+1)$-disclinations at the inclusion centre and two (-1)-disclinations at positions $x=\pm d$, respectively. When $d\ll a$ these four disclinations are virtual, situated at the centre of the inclusion and represent a quadrupole.

3.3. *Modelling with strong anchoring*

When an inclusion grows, its radius approaches a critical value associated with the hyperbolic defect appearance. This case has also to be treated for finite values of parameter Wa/B_1. However, there is no available analytical solution which can describe this case. We know two limiting solutions both composed of four (± 1)-disclinations. Solution (7) corresponds to weak anchoring when virtual disclinations are grouped near the inclusion centre. The other solution (2) with fixed anchoring also satisfies the condition (4) for infinite anchoring energy $(Wa)\to\infty$ when the condition (4) leads to $\sin 2(\Phi-\alpha)|_{r=a}=0$.

Solution (2) has a dipolar character [17] because a (-1)-disclination is outside an inclusion and the other three disclinations make an effective $(+1)$-disclination representing the inclusion. Also large inclusions having hyperbolic defects outside form a dipole. Thus we suppose that the dipolar character of the solution will dominate for inclusions exhibiting radii close to the critical. So instead of expressions (2) or (7) we propose a simple but approximate solution to describe the director orientation near such an inclusion:

$$\Phi = \alpha - \arctan\frac{(r/a)\sin\alpha}{(r/a)\cos\alpha - C}. \quad (8)$$

Again we use the parameter $C=(a+l)/a$ introduced in §3.1. The function (8) fulfils the equilibrium equation $\Delta\Phi=0$ and includes only the $(+1)$-disclination situated at the inclusion centre and representing the inclusion and the (-1)-disclination located close to the inclusion surface. It also includes a uniform **c**-director distribution at long distance. However function (8) does not take into account the equilibrium between the torques on the inclusion surface (5), and so can be used only for estimating the distance between inclusion and hyperbolic defect, or parameter C, which can be determined by the following procedure. First, by inserting

Downloaded At: 16:54 25 January 2011

equation (8) into (3) we obtain for $C \geqslant 1$:

$$W_A = -(\pi\ Wa)\left(1 - \frac{1}{2C^2}\right). \quad (9)$$

The interaction between the inclusion of topological charge (+1) and its hyperbolic defect of topological charge (−1) (figure 2) can be expressed by the elastic energy of interaction W_D along the z-axis:

$$W_D \approx \pi\ B_1 \ln \frac{C^2}{(R/a)^2} \quad (10)$$

where parameter R is the characteristic size of the film along smectic layers. The energy W_D is similar to that used for a nematic liquid crystal [14, 15, 17]. Thus the total energy W_{DA} of a defect–inclusion pair becomes:

$$W_{DA} \approx W_D + W_A \approx -(Wa\pi)\left(1 - \frac{1}{2C^2}\right) + \pi\ B_1 \ln \frac{C^2}{(R/a)^2}. \quad (11)$$

Then the minimization of (11) with respect to C leads to the dependence for the proximity coefficient:

$$C \approx \left(\frac{Wa}{2B_1}\right)^{\frac{1}{2}}. \quad (12)$$

As already mentioned, the inclusion radius a is again the only factor controlling the position of the hyperbolic defect, W and B_1 being material constants. This point has already been noted in 3D nematic systems [2, 20, 21]. The proximity coefficient C given by equation (12) increases with increasing anchoring energy Wa. However, from § 3.1 that deals with fixed (infinite) anchoring it is clear that for high values of Wa there exists an upper limit value, $C \approx \sqrt{2}$, corresponding to the rigid anchoring situation. The associated anchoring energy can be estimated: $(Wa)_{max} = 4B_1$. The value $(Wa)_{max}$ is the limiting value in our approximation: for all $Wa > (Wa)_{max}$ we define $C \approx \sqrt{2}$. On reaching the value $(Wa)_{max}$ the approximate solution (8) should be changed for the solution (2) obtained for fixed boundary conditions (infinite Wa).

Equation (12) can be helpful in interpreting the experimental behaviour of small inclusions which tend to coalesce [11]. In effect, given $C \approx 1$ for small inclusions (corresponding to a hyperbolic defect at the inclusion boundary), we can deduce from (12) a critical radius: $a_c \approx 2B_1/W$. This radius a_c discriminates two different regimes:

(i) For $a \leqslant a_c$ the anchoring energy Wa is such that no disclination is outside the inclusion. In that case, coalescence is effectively preferred.

(ii) By contrast, for $a > a_c$, the hyperbolic defect, (−1)-disclination, is outside the inclusion ($1 \leqslant C < 2$). The situation when the anchoring energy Wa is able to keep the hyperbolic defect outside the inclusion can be called the regime of strong anchoring energy.

Considering the experimental critical radius after [11], $a_c \approx 3\,\mu m$, an approximate estimation of the anchoring energy W can be calculated. The usual value for the elastic constant being $B_1 \approx 10^{-11}$ N, the estimated anchoring energy is of the order of $W \approx 6 \times 10^{-6}\,J\,m^{-2}$. When the inclusion radius is greater than the critical radius a_c, a hyperbolic defect outside the inclusion prevents the inclusion coalescence and then enables the chaining process, as will be discussed in the next section.

4. Interaction between two inclusions

Let us now consider the case of an interaction between two inclusions from having the same radius and whose hyperbolic defects are at the same distance $(a+l)$ from their respective inclusions (figure 3). This corresponds to the case of large inclusions with $C > 1$. The elastic dipole is defined as the vector relating the inclusion centre to its hyperbolic defect. It is always parallel to the **c**-director field at long distance. In [11] it was reported that hyperbolic defects are systematically located on the same side of the inclusions with respect to the uniform **c**-director orientation. This dipole configuration can be understood considering the non-invariance of the smectic C structure with respect to the $\mathbf{c} \rightarrow -\mathbf{c}$ change. This has also been mentioned by Pettey *et al.* [17]. On the other hand, the dipoles are not necessarily parallel to the lines connecting every inclusion centre called the **A**-axis. They actually make an angle ϕ with this axis (figure 3).

Using the same approach as that used in the previous section, the interaction between inclusion–defect pairs can be expressed as the interaction between (±1)-wedge disclination lines. The corresponding free energy now involves four topological charges instead of the two considered in (8):

$$\varepsilon(r, \vartheta) = \pi\ B_1 \ln \frac{\left[r^2 + (a+l)^2 - 2r(a+l)\cos\phi\right]\left[r^2 + (a+l)^2 + 2r(a+l)\cos\phi\right]}{r^4}. \quad (13)$$

Expression (13) describes the interactions induced by the spatial **c**-director gradient. This interaction energy $\varepsilon(r, \phi)$ is of dipolar type at long range $(a+l) \ll r$. Indeed it can be easily verified that its expansion versus $(a+l)/r$ leads to an $1/r^2$ dependence: $\varepsilon(r, \phi) \approx 2\pi B_1(1 - 2\cos^2\phi)[(a+l)/r]^2$.

Downloaded At: 16:54 25 January 2011

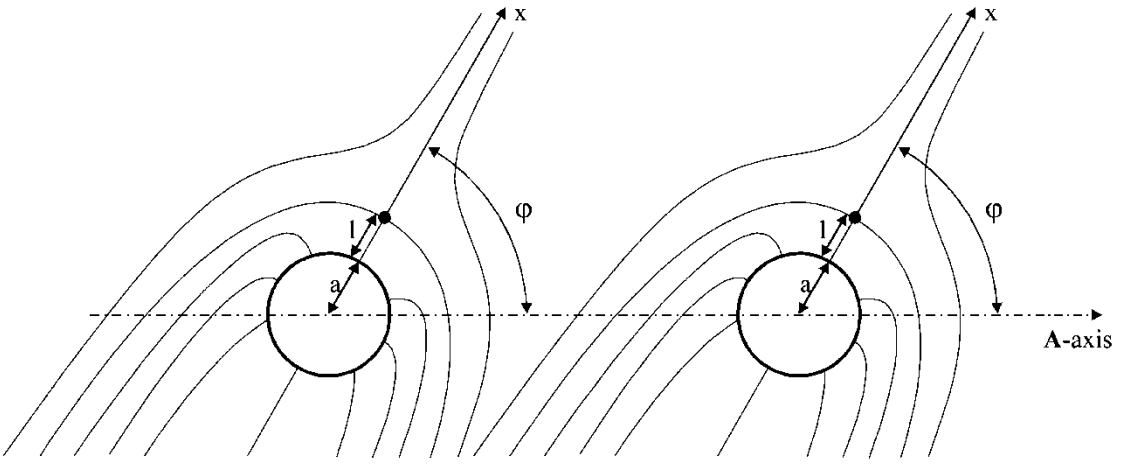

Figure 3. Two identical inclusions with distance r between their centres and their accompanying hyperbolic defects. The **A**-axis connects the inclusion centres. Dipole axes lie along the x-axis, making an angle ϕ with the **A**-axis. The solid lines visualize the **c**-director field.

Downloaded At: 16:54 25 January 2011

4.1. *Dipolar angle condition for inclusion chaining*

The radial force (per unit length in the z-direction) acting on the inclusions can be derived from expression (13):

$$F_r = -\frac{\partial \varepsilon(r,\phi)}{\partial r} = 4\pi B_1 \frac{(a+l)^2\left[(a+l)^2 + r^2\left(1-2\cos^2\phi\right)\right]}{\left\{\left[r^2+(a+l)^2\right]^2 - 4r^2(a+l)^2\cos^2\phi\right\}}. \quad (14)$$

The radial force (14) is attractive when angle ϕ satisfies the condition (15):

$$\frac{1}{2}\left[\frac{(a+l)^2}{r^2}+1\right] < \cos^2\phi. \quad (15)$$

Strictly the **A**-axis (figure 3) has a meaning only when two inclusions are present in the film, since its purpose is to relate their centres. When that condition is fulfilled, the angle ϕ determines the position of the associated inclusion dipoles with respect to the **A**-axis.

Let us take a fixed inclusion at position $r=0$ as reference and then consider another inclusion which is nucleated or positioned far from the reference one, i.e. with $(a+l) \ll r$. According to equation (15), both inclusions tend to attract one another for any angle ϕ within the intervals $\phi \in (-\pi/4, \pi/4)$ or/and $\phi \in (3\pi/4, 5\pi/4)$. Then a chain can possibly be formed. For angles outside these intervals, force (14) becomes repulsive. So, starting from a random location of the inclusion at the time of nucleation, the angular dependence of the radial force allows us to explain the final distribution of the inclusions into an array of parallel chains.

Considering now the interaction between two already formed chains that are parallel and not too far from each other, we deduce from equation (14) that they tend to repel one another when the angle ϕ has values near $\pi/2$. Such behaviour is fully confirmed by the experimental observations (see figure 4). Figure 4 shows that the self-organization of inclusions in a film exhibiting a long-range uniform **c**-director field, leads to a quasi-regular array of parallel chains of inclusions. The inclusions from neighbouring parallel chains repel each other at short distances when ϕ is close to $\pi/2$, stabilizing the chain at an equilibrium distance.

4.2. *Rotation of the elastic dipoles*

During the final part of the chaining process, experimental observations (see figure 5) have shown a rotation

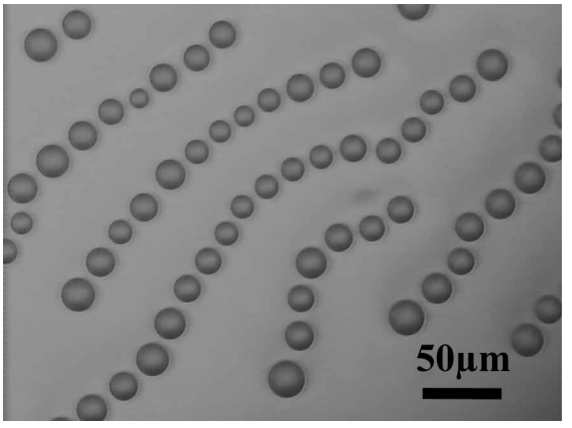

Figure 4. Microscope image of an array of nearly parallel chains of droplets (associated hyperbolic defects are not visible because there are no polarizers). No lateral chaining is observed.

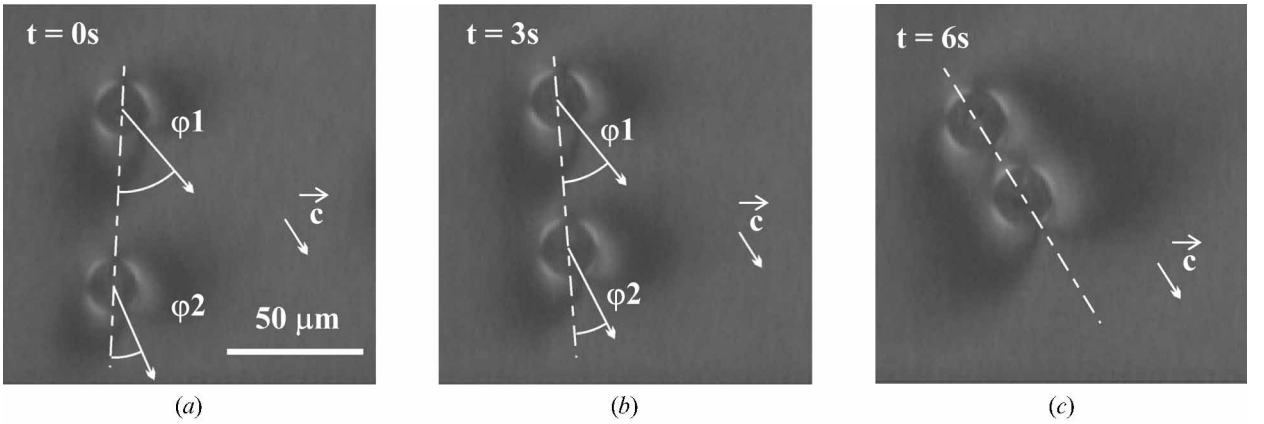

Figure 5. Attraction of two inclusions. The three photomicrographs give the evolution of the angle ϕ during chaining process: (*a*) $\phi 1 = 45°$, $\phi 2 = 27°$; (*b*) $\phi 1 = 35°$, $\phi 2 = 22°$; (*c*) $\phi 1 = \phi 2 = 0$. The **A**-axis (dashed line relating the inclusion centres) slowly rotates until it becomes parallel to **c**. The elastic dipoles of both inclusions (represented by arrows) remain along the average **c**-director field at long distance during the chaining process.

of the **A**-axis along the dipoles direction (i.e. ϕ tending to zero). This behaviour can be understood by investigating the angular force behaviour, associated with the interaction energy (13):

$$F_\phi = -\frac{\partial \varepsilon(r,\phi)}{r\partial\phi} = -4\pi B_1 \frac{r(a+l)^2 \sin 2\phi}{\left\{\left[r^2+(a+l)^2\right]^2 - 4r^2(a+l)^2\cos^2\phi\right\}}. \quad (16)$$

Equilibrium positions resulting from $F_\phi = 0$ give the angle values $\phi = 0$ and $\phi = \pi/2$. The stable angle orientation is given by a chain parallel to the **c**-director ($\phi = 0$), whereas a chain perpendicular to it is unstable ($\phi = \pi/2$).

Figure 5 illustrates well the different steps followed during the inclusions chaining: (i) elastic dipoles of both inclusions remain along the average **c**-director field at long distance during the chaining process; (ii) the **A**-axis (dashed line relating the inclusion centres) slowly rotates until becoming parallel to the **c**-director field when the inclusions reach their equilibrium distance. The angular dependence of the radial and angular interaction forces can fully explain the experimental behaviour of inclusions illustrated by figures 4 and 5. Thus, in most cases the final distribution of the inclusions leads to the formation of a nearly periodic system exhibiting parallel chains lying along the **c**-director.

4.3. *Proximity coefficient for the 'two-inclusions' chain*

In order to estimate the proximity coefficient $C = (a+l)/a$ associated with a chain built with two inclusions, we need to add a term expressing the repulsion between the topological charges of both inclusions and their associated defects. Then expression (11) for energy with finite anchoring becomes:

$$W_{\mathrm{DA}}^{\mathrm{int}} \approx 2\pi\, B_1 \ln\frac{C^2}{(R/a)^2} - \pi\, B_1 \ln\frac{4C^2}{(R/a)^2} - 2(Wa\pi)\left(1-\frac{1}{2C^2}\right). \quad (17)$$

The minimization of (17) gives:

$$C_{\mathrm{int}} \approx \left(\frac{Wa}{B_1}\right)^{\frac{1}{2}}. \quad (18)$$

The resulting proximity coefficient (18) is similar to that obtained for an isolated inclusion except it is $\sqrt{2}$ greater. The exact analysis of this problem should be performed numerically, as was demonstrated in the case of two inclusions for fixed anchoring conditions in [18].

We note that experimental studies [11] have clearly shown that the proximity coefficient depends also on the film thickness. The modelling of the effect of thickness is currently under study.

5. Contributions of chirality

In previous experimental investigations we found that in SmC* films, the **c**-director anchoring is radial whereas it is tangential in non-chiral SmC films [11, 12]. Thus, the chirality seems to influence the type of director anchoring at the inclusion boundaries.

In the chiral smectic structure, the spontaneous polarization is parallel to the smectic layers and perpendicular to the **c**-director [15]. The charge associated with the polarization divergence around the inclusions can increase their interaction energy. Thus, we can reasonably suppose that the **c**-director adopts a radial

Downloaded At: 16:54 25 January 2011

configuration around the inclusions in order to minimize the polarization charge effect. The spontaneous polarization is thus tangential to the inclusion surface, leading to a global zero electrical charge around the inclusion. We can also expect that the anchoring energy will be high for materials with high values of spontaneous polarization.

As for the hyperbolic defect, it can also carry a non-zero charge in chiral-smectic films. Such influences, linked to spontaneous polarization, must be taken into account for a more detailed study of inclusion chaining.

6. Conclusions

We have proposed a simplified model describing the interactions between an isolated inclusion with its hyperbolic defect as well as the interactions between two inclusions during their chaining. The model enables us to explain the main types of behaviour reported in our previous experimental studies of SmC* chiral films at the SmC*–N* transition [9, 11].

Each inclusion and its associated hyperbolic defect are modelled as a pair of (± 1)-wedge disclination lines. It is then possible to relate the distance between the inclusion and its hyperbolic defect to its radius, thanks to the introduction of a finite anchoring energy in the interaction energy of the system. A critical radius can also be deduced below which the topological hyperbolic defect becomes virtual. Such characteristics shine some light on the coalescence process observed experimentally for the smallest inclusions.

As for the interaction involving two inclusion–defect pairs, the attractive or repulsive nature of the interaction forces is directly dependent on the angle of the elastic dipole axis with respect to that connecting the inclusion centres. The equilibrium state is reached when this angle is zero, which corresponds effectively to the formation of a chain parallel to the **c**-director. Our model also explains why the inclusions organize themselves in parallel chains. The separation of two adjacent inclusions in a chain is shown to be greater than twice the distance between inclusion and defect in the isolated situation.

Further investigations will be made to evaluate the influence of chirality on the inclusion elastic interaction energy. The first parameter to be taken into account will be the spontaneous polarization in the smectic chiral film. The second parameter will be the helical pitch, which cannot always be neglected for the thickest smectic chiral films. Another interesting aspect to study will concern the dependence of the inclusion–inclusion separation as a function of film thickness.

L.L. would like to thank the Laboratoire de Dynamique et Structure des Matériaux Moléculaires at Université de Lille I for hospitality. This work was also supported by Grant No. 202/02/0840 of the Grant Agency of the Czech Republic and by the research project AV0Z1-010-914. We thank the Région Nord-Pas de Calais and FEDER for funding of the image set-up.

References

[1] Poulin, P., Stark, H., Lubensky, T. C., and Weitz, D. A., 1997, *Science*, **275,** 1770.
[2] Loudet, J.-C., Barrois, P., and Poulin, P., 2000, *Nature*, **407,** 611.
[3] Poulin, P., and Weitz, D. A., 1998, *Phys. Rev. E*, **57,** 626.
[4] Nazarenko, V. G., Nych, A. B., and Lev, B. I., 2001, *Phys. Rev. Lett.*, **87,** 075 504/1.
[5] Lubensky, T. C., Pettey, D., Currier, N., and Stark, H., 1998, *Phys. Rev. E*, **57,** 610.
[6] Ruhwandl, R. W., and Terentjev, E. M., 1997, *Phys. Rev. E*, **56,** 5561.
[7] Stark, H., 1999, *Eur. Phys. J. B*, **10,** 311.
[8] Poulin, P., Cabuil, V., and Weitz, D. A., 1997, *Phys. Rev. Lett.*, **79,** 4862.
[9] Cluzeau, P., Dolganov, V., Poulin, P., Joly, G., and Nguyen, H. T., 2001, *Mol. Cryst. Liq. Cryst.*, **364,** 381.
[10] Cluzeau, P., Poulin, P., Joly, G., and Nguyen, H. T., 2001, *Phys. Rev. E*, **63,** 031 702/1.
[11] Cluzeau, P., Bonnand, V., Joly, G., Dolganov, V., and Nguyen, H. T., 2003, *Eur. Phys. J. E*, **10,** 231.
[12] Cluzeau, P., Joly, G., Nguyen, H. T., and Dolganov, V. K., 2002, *JETP Lett.*, **75,** 482.
[13] Cluzeau, P., Ismaili, M., Anakkar, A., Foulon, M., Babeau, A., and Nguyen, H. T., 2001, *Mol. Cryst. liq. Cryst.*, **362,** 185.
[14] Kléman, M., 1983, *Points, Lines, and Walls in Liquid Crystals, Magnetic Systems and Various Ordered Media* (New York: Wiley).
[15] De Gennes, P. G., and Prost, J., 1993, *The Physics of Liquid Crystals*, 2nd Edn (Oxford: Oxford University Press).
[16] Glogarová, M., Lejček, L., Pavel, J., Janovec, V., and Fousek, J., 1983, *Mol. Cryst. Liq. Cryst.*, **91,** 309.
[17] Pettey, D., Lubensky, T. C., and Link, D. R., 1998, *Liq. Cryst.*, **28,** 579.
[18] Patricio, P., Tasinkevych, M., and Telo da Gama, M. M., 2002, *Eur. Phys. J. E*, **7,** 117.
[19] Oswald, P., and Pieranski, P., 2000 and 2002, *Les Cristaux Liquides*, Vols. 1 and 2 (Paris: Gordon and Breach).
[20] Terentjev, E. M., 1995, *Phys. Rev E*, **51,** 1330.
[21] Kuksenok, O. V., Ruhwandl, R. W., Shiyanovskii, S. V., and Terentjev, E. M., 1996, *Phys. Rev. E*, **54,** 5198.
[22] Fukuda, J., and Yokoyama, H., 2001, *Eur. Phys. J. E*, **4,** 389.

Downloaded At: 16:54 25 January 2011